RSC Advances

PAPER

View Article Online
View Journal | View Issue

Check for updates

Cite this: *RSC Adv.*, 2025, **15**, 9467

Ethylene oligomerization to liquid fuels over steam and phosphorus modified MFI zeolites†

Fuchao Li, Jianqiang Liu, Enhui Xing, Xiaoli Wei, Jianhong Gong,* Yibin Luo* and Xingtian Shu

A series of steam and phosphorus modified ZSM-5 samples were prepared to investigate the effect of pore structure and acid property on ethylene oligomerization. Characterization results showed that steam treatment contributed to generate mesopores with pore sizes of 2–3 nm and 10–20 nm, while progressive aggregation of phosphorus species on the exterior surface resulted in blockage of channels. Dealumination of framework aluminum led to a gradual decline in total acidity and acid strength with an increase of steam temperature or P/Al ratio. Sufficient strong acid sites and enhanced accessibility to the inner active sites were crucial factors in conversion of ethylene to liquid fuels. The steam modified sample at 700 °C (HZ-700) obtained the highest yield of liquid fuels up to 78.1%, which demonstrated an increase of 40% in comparison with the unmodified sample. Due to improved diffusional capacity originating from mesopores, HZ-700 showed a higher deactivation stability than the phosphorus modified sample at similar conversion levels. This work will provide some insight into the development of zeolite-based catalyst for ethylene oligomerization to liquid fuels.

Received 27th February 2025
Accepted 23rd March 2025

DOI: 10.1039/d5ra01413a

rsc.li/rsc-advances

Open Access Article. Published on 28 March 2025. Downloaded on 12/14/2025 8:48:57 AM.
This article is licensed under a Creative Commons Attribution-NonCommercial 3.0 Unported Licence.

1. Introduction

Oligomerization of ethylene and other light olefins (C_3–C_6), is a key step for producing linear and branched olefins, which are widely applied in synthesis of valuable products such as petrochemicals, transportation fuels, detergents and lubricant additives.[1–3] In order to mitigate the environmental impact of the current reliance on petroleum-derived fuels, ethylene oligomerization to liquid fuels has attracted more attention, especially when ethylene can be obtained from renewable bio-based ethanol.[4,5] The industrial-scale processes for ethylene oligomerization are typically catalyzed by homogeneous catalysts comprising a transition metal (mainly nickel) complex activated by an alkyl-aluminum co-catalyst.[6,7] However, homogeneous catalysis suffers from several problems, including harsh reaction conditions, the instability of the solvent, and the difficulty in recycling the catalyst from the reaction products.[3,8]

In this regard, heterogeneous catalysis is an environmentally friendly alternative to the homogenous process. Tremendous efforts have been made into the search for highly active and selective bifunctional catalysts with Ni ions loaded on a range of acid aluminosilicates, such as amorphous silica-alumina,[9,10] microporous HZSM-5 zeolite,[11,12] nanocrystalline beta zeolite,[13] ordered mesoporous material SBA-15,[14] MCM-41,[15] and KIT-6 (ref. 16) in the past decades. With regard to liquid fuels, a major challenge associated with these Ni-supported catalysts is the low selectivity toward the higher branched oligomers due to the limitation of typical Schulz–Flory distribution ($C_4 > C_6 > C_8 > C_{10+}$).[17,18] Furthermore, nickel species are relatively stable at low temperatures,[19] while ethylene oligomerized at a higher deactivation rate over the Ni-modified catalyst in the temperature range of 300–400 °C.[20]

Therefore, the excellent thermal stability of nickel-free zeolite has been widely applied as the oligomerization catalyst to produce liquid fuel. ZSM-5 zeolite with medium pore system has shown remarkably superior activity in ethylene oligomerization, but confronted with low selectivity towards C_{5+} products and high tendency to coke deactivation.[21,22] To improve catalytic performance and enhance the selectivity to liquid fuels, the pore structure and acidity of the ZSM-5 zeolite should be carefully tailored with post-synthesis modification. Steam and phosphorus modification are common strategies to adjust the acidity of the zeolites and have been used in industrial applications. The stability of the ZSM-5 catalyst was significantly enhanced in methanol conversion reactions with an increase of light olefins selectivity due to decreasing acidity by steam treatment.[23,24] Triantafillidis *et al.*[25] reported that numerous pores with sizes in the range of 5–20 nm can be effectively presented and significant amounts of extra-framework phases were formed after a severe steam treatment at 790 °C for 6 h. In addition, due to a change in the acid strength distribution, phosphorus modified HZSM-5 zeolites could enhance the selectivity to propylene but decreased the conversion of

State Key Laboratory of Petroleum Molecular and Process Engineering, Research Institute of Petroleum Processing, Sinopec, Beijing 100083, China. E-mail: gongjh.ripp@sinopec.com; luoyibin.ripp@sinopec.com

† Electronic supplementary information (ESI) available. See DOI: https://doi.org/10.1039/d5ra01413a

© 2025 The Author(s). Published by the Royal Society of Chemistry

Open Access Article. Published on 28 March 2025. Downloaded on 12/14/2025 8:48:57 AM. This article is licensed under a Creative Commons Attribution-NonCommercial 3.0 Unported Licence.

ethylene.[26] Janardhan *et al.*[27] found that ZSM-5 by phosphate treatment generated new kinds of acid sites accompanied with a narrow pore diameter, which selectively catalyzed alkylation and contributed to a higher selectivity towards targeted *para*-xylene product. However, the difference between steam and phosphorus modification on the textural and acidity property of ZSM-5 zeolite has not been systematically investigated in ethylene oligomerization to liquid fuels.

In this work, a series of ZSM-5 samples were prepared by steam and phosphorus modification and their performance in ethylene oligomerization was tested. The physical and acidity properties of unmodified and modified ZSM-5 samples were comprehensively characterized. The results suggest that steam and phosphorus modification are effective methods to alter textural structure, acidity and distribution of acid sites. Due to newly generated mesoporous structure, steam modified ZSM-5 samples could obtain a higher yield of liquid products and a lower coke content in comparison with the phosphorus treated sample at similar conversion level. In addition, the relationship between catalyst structure and oligomerization performance was also investigated.

2. Experimental

2.1 Catalyst preparation

Commercially available HZSM-5 zeolite (SiO_2/Al_2O_3 molar ratio = 26.4, denoted as HZ) was provided by Sinopec Qilu Catalyst Company. Ammonium phosphate dibasic ($H_9N_2O_4P$, 99.9%) was purchased from Aladdin Industrial Corporation, and used without further purification.

2.1.1 Steam modification of ZSM-5. The 10.0 g of the HZ sample with sizes of 20–40 mesh was loaded in a vertical tubular reactor. The catalyst was preheated from room temperature to the selected temperature under air flow (100 mL min^{-1}) for 2 h before the continuous stream with a flow rate of 1.5 mL min^{-1} for 4 h. The selected temperature was 600, 700, 750 and 800 °C, respectively. The resulting samples were denoted as HZ-*X*, where *X* represented the steam temperature.

2.1.2 Phosphorus modification of ZSM-5. The phosphorus modification of HZSM-5 was conducted by incipient wet impregnation using an aqueous solution of ammonium phosphate dibasic at room temperature with liquid-to-solid mass ratio of 1.5. The targeted P/Al molar ratio was set as 0.5, 1.0 and 1.5, respectively. The slurry was dried overnight at 120 °C and then calcined at 550 °C for 3 h. The final samples were labeled as PZ-*Y*, where *Y* represented the P/Al ratio.

2.2 Catalysts characterization

The crystalline structures of zeolites were investigated by X-ray diffraction (XRD) patterns over a Panalytical Empyrean diffractometer with Cu Kα (λ = 0.154 nm) radiation. The instrument was operated at 40 kV, 250 mA. The scanning range was from 5 to 50°. A Rigaku ZSX100E X-ray fluorescence (XRF) spectrometer was applied to analyze the bulk chemical composition of the catalysts. The X-ray photoelectron spectroscopy (XPS) experiments were performed using a Thermo Fisher ESCALAB Xi^+ electron spectrometer with 150 W monochromatic Al K_α radiation. The narrow scans were acquired for elemental core levels with a pass energy of 30 eV to produce high-resolution spectra. The binding energy was calibrated using C 1s peak at 284.8 eV. The textural properties of the samples were characterized by nitrogen physisorption at 77 K on a Micromeritics ASAP 2460 analyzer. The total surface area was calculated by the Brunauer–Emmett–Teller (BET) equation. Transmission electron microscope (TEM) images were recorded on FEI TECNAIGF20 transmission electron microscope operating at 200 kV.

NH_3-TPD characterization was carried out on a Micromeritics AutoChem II 2920 instrument. NH_3 desorption was conducted from 150 to 600 °C at a heating rate of 10 °C min^{-1} under a He flow. The total acidity was obtained by deconvolution of NH_3-TPD curves. The concentrations of Brønsted and Lewis (abbreviated as B and L, respectively) acid sites were determined by IR spectroscopy using pyridine as probe molecule on a spectrometer (BIO-RAD FTS3000). The sample was activated at 450 °C for 120 min in vacuum system and then saturated with pyridine. The spectrum of the sample at 200 °C and 350 °C was collected during the cooling process. Solid-state magic angle spinning nuclear magnetic resonance (MAS NMR) characterization was performed on a Bruker Advance III 600WB spectrometer. The ^{27}Al MAS NMR spectra were recorded at a resonance frequency of 156.4 MHz by using a 4 mm probe at a spinning rate of 10 kHz. The chemical shift of ^{27}Al was referenced to 1 M aqueous $Al(NO_3)_3$. The ^{31}P MAS NMR spectra were recorded at 202.4 MHz using a 4 mm probe under magic-angle spinning speed of 5 kHz. The chemical shift of ^{31}P was referenced to $(NH_4)_2HPO_4$. Thermogravimetric analysis (TG) of the spent catalysts was performed on a SDT Q600 thermal analyzer from room temperature to 800 °C with a heating rate of 10 °C min^{-1} in air atmosphere. The amount of coke deposit was calculated by weight loss from 200 to 800 °C.

2.3 Oligomerization of ethylene

Ethylene oligomerization was performed in a continuous fixed-bed reactor at 300 °C, 20 bar, and weight hourly space velocity of 1.0 h^{-1} with catalyst loading weight of 6.0 g. The reactor was a stainless steel tube with an internal diameter of 16 mm and a total length of 0.7 m. The samples were pelletized, crushed, and sieved to recover the particle fraction with sizes of 20–40 mesh. Prior to the oligomerization experiments, the catalyst was pre-treated with a N_2 flow (100 mL min^{-1}) under atmospheric pressure at 500 °C for 2 h. Then, the reactor was cooled down to the desired reaction temperature with a N_2 flow (150 mL min^{-1}) and the total pressure was increased to 20 bar. Afterwards, the N_2 flow was stopped and the feed mixture comprising 39.7 mol% ethylene and 60.3 mol% Ar was fed into the reactor. Unconverted reactant and non-condensable reaction products sampled at periodic intervals, were analyzed off-line on a gas chromatograph (Agilent 7890B) equipped with a capillary column (HP-AL/S, 25 m × 0.32 mm × 0.5 μm), two packed columns (Porapak Q and molecular sieve 13×), a FID and two TCD detectors. The liquid products, condensed in cold traps at −3 °C, were collected at the end of the runs, weighed and

 © 2025 The Author(s). Published by the Royal Society of Chemistry

Open Access Article. Published on 28 March 2025. Downloaded on 12/14/2025 8:48:57 AM. This article is licensed under a Creative Commons Attribution-NonCommercial 3.0 Unported Licence.

analyzed by another gas chromatograph (Agilent 7890A) with a capillary column (HP-PONA, 50 m × 0.2 mm × 0.5 μm) using a FID detector.

The instantaneous conversion of ethylene (X_t, mol%) at a given time on stream (TOS) is calculated by the following formula

$$X_t = \left(1 - \frac{C_{ethylene,out} C_{Ar,in}}{C_{ethylene,in} C_{Ar,out}}\right) \times 100\%$$

where $C_{ethylene,out}$ and $C_{Ar,out}$ are the concentrations of ethylene and Ar at the reactor outlet as measured by the gas chromatograph, and $C_{ethylene,in}$ and $C_{Ar,in}$ denote the concentrations of ethylene and Ar in the feed mixture, respectively.

The formulas for calculating the average ethylene conversion (X_A, wt%), product selectivity (S_i, wt%) and yield (Y, wt%) are defined as follows

$$X_A = \left(1 - \frac{m_1}{m_0}\right) \times 100\%$$

$$S_i = \left(\frac{m_i}{m_0 - m_1}\right) \times 100\%$$

$$Y_i = X_A \times S_i$$

where m_0 is the mass of ethylene in the feed, m_1 and m_i are the mass of ethylene and each i product in the product stream, respectively.

3. Results and discussion

3.1 Catalyst characterization

The XRD patterns of steam and phosphorus modified ZSM-5 samples are displayed in Fig. 1. The characteristic diffraction peaks assigned to MFI topology at 2θ of 7.9°, 8.8°, 23.0°, 23.8° and 24.4° (ref. 28) can be observed over the pristine and modified samples and no impurity phases were detected. As shown in Table 1, there is a slight decline in the crystallinity of steam modified samples when steam temperature increased, and the relative crystallinity of HZ-800 sample was up to 91.0%. However, the relative crystallinity significantly dropped from 88.7% for PZ-0.5 to 67.3% for PZ-1.5, suggesting an obvious loss of the crystallinity over the phosphorus modified samples, which was ascribed to the substantial loading of phosphorus species.

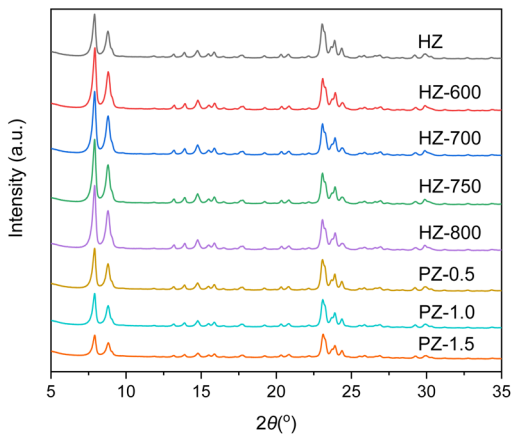

Fig. 1 XRD patterns of steam and phosphorus modified ZSM-5 samples.

XRF and XPS analysis were deployed to provide detailed information on chemical composition of steam and phosphorus modified ZSM-5 samples. As listed in Table 1, a slight decline in the SiO_2/Al_2O_3 ratio was observed for steam modified ZSM-5 samples as the steam temperature increased. The SiO_2/Al_2O_3 ratio of HZ and HZ-800 was 26.4 and 25.6, respectively. Phosphorus modification exhibited negligible influence on the SiO_2/Al_2O_3 ratio. In addition, the surface P/Al ratio of phosphorus modified ZSM-5 samples was higher than that of the bulk counterpart. The discrepancy between surface and bulk P/Al ratio became more pronounced with an increase in phosphorus content. The surface and bulk P/Al ratio for PZ-1.5 sample was 2.18 and 1.51, respectively, indicating progressive aggregation of phosphorus species on the exterior surface due to the diffusion limitations toward the interior zeolite channels.[29]

The textural properties of steam and phosphorus modified ZSM-5 samples were investigated from N_2 adsorption–desorption isotherms. As shown in Fig. 2a, the pristine HZ sample showed a mixture of IUPAC type-I and type-IV isotherms with a small hysteresis loop closed in the range of $0.5 < P/P_0 < 1.0$, revealing the presence of mesoporous structure over the commercial ZSM-5 zeolite. After steam treatment at 600 °C, a noticeable change in the hysteresis loop at the P/P_0 of 0.45–1.0 can be observed. Further increasing steam temperature to 700–800 °C, the hysteresis loop became larger and shifted to wider position with P/P_0 in the range of 0.15–1.0. This suggested that more mesopores with a larger diameter were generated after steam modification at higher temperatures.[30] Pore size distribution in Fig. 2b confirmed that mesopores with pore diameter of 2–3 nm and 10–20 nm were newly created over steam treated samples and the pore size steadily enlarged as the temperature increased. From Fig. 2c, compared with the pristine HZ, the hysteresis loop became smaller and a decline in N_2 uptake can be detected over phosphorus modified ZSM-5 samples with an increase of P/Al ratio. The pore centered at 4 nm was attributed to the secondary pore formed by deposition of phosphorus species (Fig. 2d).

As summarized in Table 1, the pristine HZ sample had a specific surface area of 367 $m^2\ g^{-1}$ and a total volume of 0.207 $cm^3\ g^{-1}$ with the micropore volume of 0.154 $cm^3\ g^{-1}$, indicated a characteristic microporous structure. With increasing steam temperature, a gradual decline in the BET surface area, micropore surface and micropore volume can be observed, which was mainly related to the loss of micropore under steam conditions. The pore volume and mesopore volume of steam modified ZSM-5 samples exhibited an increase, followed by a subsequent decrease. It should be noted that HZ-700 sample presented the maximum mesopore volume (0.081 $cm^3\ g^{-1}$) with a high total

Open Access Article. Published on 28 March 2025. Downloaded on 12/14/2025 8:48:57 AM. This article is licensed under a Creative Commons Attribution-NonCommercial 3.0 Unported Licence.

Table 1 Textural properties and chemical composition of steam and phosphorus modified ZSM-5 samples

Sample	R.C.[a]	SiO_2/Al_2O_3[b]	P/Al		S_{BET} ($m^2\ g^{-1}$)	S_{micro} ($m^2\ g^{-1}$)	V_{total} ($cm^3\ g^{-1}$)	V_{micro} ($cm^3\ g^{-1}$)	V_{meso} ($cm^3\ g^{-1}$)
			Bulk[b]	Surface[c]					
HZ	100	26.4	—	—	367	331	0.207	0.154	0.053
HZ-600	94.2	26.5	—	—	330	288	0.216	0.141	0.076
HZ-700	93.6	26.2	—	—	310	264	0.215	0.134	0.081
HZ-750	92.5	26.0	—	—	306	266	0.213	0.139	0.076
HZ-800	91.0	25.6	—	—	299	255	0.213	0.134	0.079
PZ-0.5	88.7	25.9	0.49	0.59	282	254	0.169	0.118	0.051
PZ-1.0	79.3	25.8	1.11	1.18	225	203	0.133	0.094	0.039
PZ-1.5	67.3	26.2	1.51	2.18	168	156	0.101	0.072	0.030

[a] Relative crystallinity. [b] Molar ratio measured by XRF. [c] Molar ratio measured by XPS.

volume (0.215 $cm^3\ g^{-1}$). As the phosphorus loading increased, the BET surface area, micropore surface, total volume and micropore volume all decreased significantly. The BET specific area (168 $m^2\ g^{-1}$) and total volume (0.101 $cm^3\ g^{-1}$) of the PZ-1.5 sample were considerably lower in comparison with those of the HZ-26 zeolites, which was attributed to the pore blockage by accumulated phosphorus species.[31]

The TEM images in Fig. S1† further showed the textural changes of steam and phosphorus modified ZSM-5 samples. The pristine HZ sample presented purely microporous structure and a smooth surface with well-defined edges. After steam treatment, sponge-like structure with round voids or hollow features was clearly observed over the HZ-700 sample, demonstrating the generation of mesopores. In addition, the surface of the PZ-1.0 sample became rough due to an agglomeration of phosphorus species.

The acidic properties of steam and phosphorus modified ZSM-5 samples were studied by NH_3-TPD and the curves are

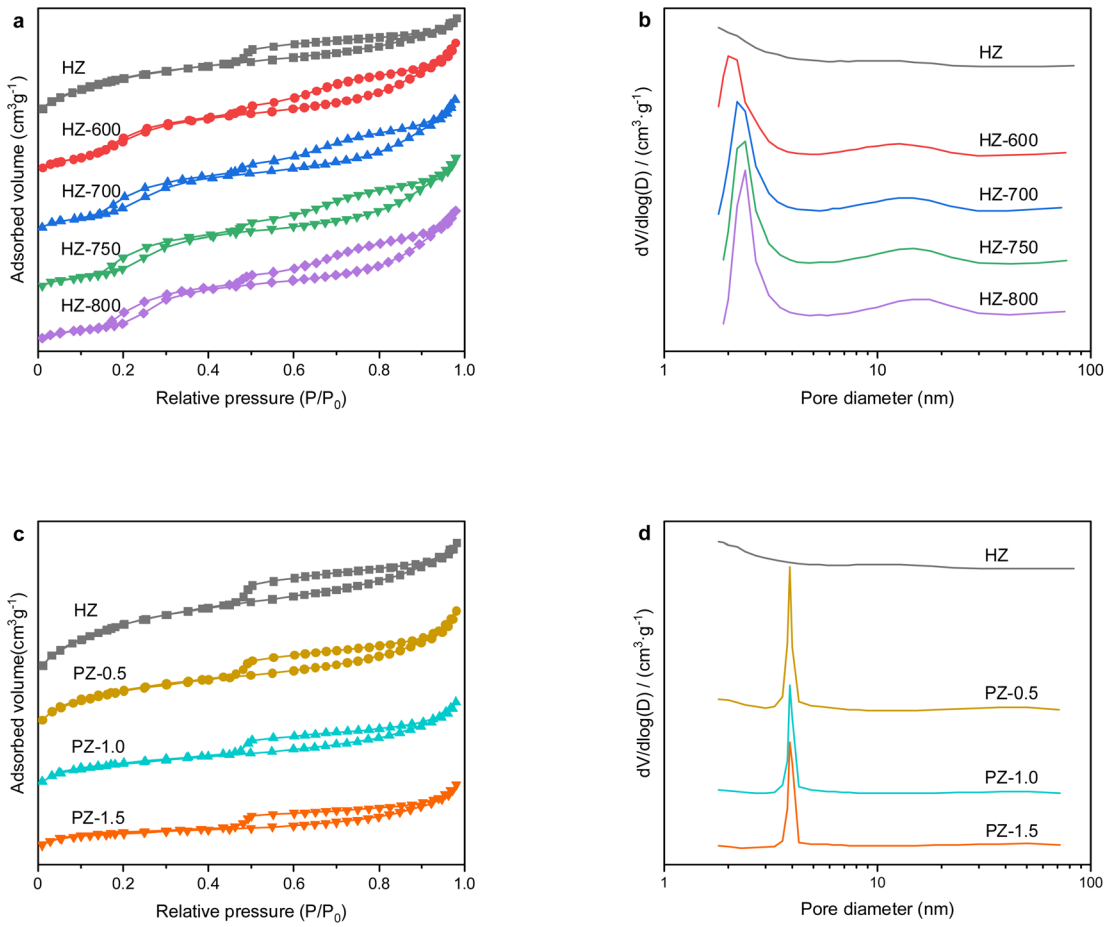

Fig. 2 N_2 adsorption–desorption isotherms and pore size distribution of (a and b) steam and (c and d) phosphorus modified ZSM-5 samples.

© 2025 The Author(s). Published by the Royal Society of Chemistry

Open Access Article. Published on 28 March 2025. Downloaded on 12/14/2025 8:48:57 AM.
This article is licensed under a Creative Commons Attribution-NonCommercial 3.0 Unported Licence.

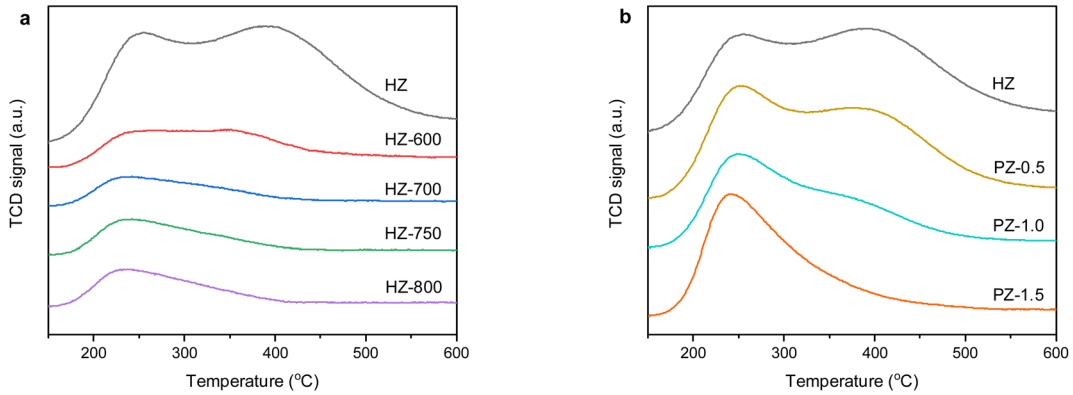

Fig. 3 NH_3-TPD curves of (a) steam and (b) phosphorus modified ZSM-5 samples.

presented in Fig. 3. Two characteristic NH_3 desorption peaks centered at around 250 and 400 °C were observed over the pristine HZ sample. Generally, the low temperature desorption peak is assigned to weak acid sites, while the high temperature desorption peak corresponds to the strong acid sites.[32] After steam treatment, both the high-temperature and low-temperature desorption peaks decreased remarkably as shown in Fig. 3a. When the steam temperature was higher than 700 °C, the high-temperature desorption peak almost disappeared. At the same time, the low-temperature desorption peak shifted to a relatively lower temperature, from 250 to 230 °C, indicating a significant decrease in acid amount and strength of steam modified ZSM-5 samples, especially for strong acid sites. From Fig. 3b, the phosphorus modified ZSM-5 samples showed a behavior of acid property similar to that of steam modified samples. The high-temperature desorption peak nearly faded away when the P/Al ratio was higher than 1.0. The low-temperature desorption peak can be preserved to a larger extent, with a slight decrease in the desorption temperature to 240 °C. The integrated results of NH_3-TPD curves are listed in Table 2. Compared to the pristine HZ sample with a total acidity of 810.6 μmol g^{-1}, a notable decrease in total acidity of steam modified ZSM-5 samples was observed with the increase of steam temperature. The HZ-800 sample had the lowest total acidity of 72.3 μmol g^{-1}. Moreover, the PZ-1.5 sample showed the smallest total acidity of 219.2 μmol g^{-1} among the phosphorus modified samples.

The amounts and distribution of Brønsted and Lewis acid sites of steam and phosphorus modified ZSM-5 samples were further characterized by IR spectroscopy using pyridine as probe molecule. The acid amount is calculated based on Emeis's equation[33] and listed in Table 2. After steam modification, a sharp drop in the amount of Brønsted and Lewis acid sites was observed, and the B/L ratio exhibited an obvious decline with the increase of steam temperature. This indicated that the Brønsted acid sites were more susceptible to the influence of steam treatment compared to the Lewis acid sites. It is worthy noted that the strong Brønsted and Lewis acid sites could not be detected over the HZ-750 and HZ-800 samples, which were in agreement with the NH_3-TPD results. In addition, phosphorus modified ZSM-5 samples presented a gradual decline in the amount of Brønsted and Lewis acid sites as the P/Al ratio increased. The PZ-1.5 sample exhibited a negligible quantity of strong Brønsted and Lewis acid sites, corresponding to the results by NH_3-TPD.

The ^{27}Al MAS NMR spectra of steam modified ZSM-5 samples are provided in Fig. 4a. The pristine HZ sample showed an intense resonance at 55 ppm and a small resonance at 0 ppm,

Table 2 Acid properties of steam and phosphorus modified ZSM-5 samples

		Amount (μmol g^{-1}) of total acid sites[b] (200 °C)			Amount (μmol g^{-1}) of strong acid sites[b] (350 °C)		
Sample	Total acidity[a] (μmol g^{-1})	B	L	B/L	B	L	B/L
HZ	810.6	223.9	99.8	2.2	156.2	67.0	2.3
HZ-600	256.1	28.3	21.8	1.3	8.0	10.1	0.8
HZ-700	146.0	7.4	14.7	0.5	0.5	3.4	0.1
HZ-750	96.3	5.1	6.3	0.8	0	0	—
HZ-800	72.3	0	3.8	0	0	0	—
PZ-0.5	509.7	115.7	38.4	3.0	57.3	23.3	2.5
PZ-1.0	307.3	54.9	7.6	7.3	9.8	2.6	3.8
PZ-1.5	219.2	21.0	2.6	8.1	0.8	0	—

[a] Total acidity measured by NH_3-TPD. [b] The amounts of total and strong acid sites determined by pyridine-adsorbed IR.

Open Access Article. Published on 28 March 2025. Downloaded on 12/14/2025 8:48:57 AM.
This article is licensed under a Creative Commons Attribution-NonCommercial 3.0 Unported Licence.

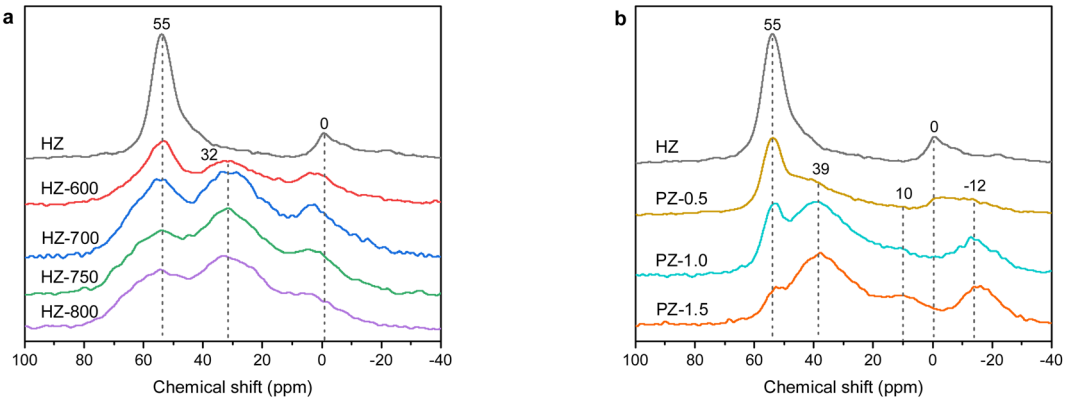

Fig. 4 ^{27}Al MAS NMR spectra of (a) steam and (b) phosphorus modified ZSM-5 samples.

which were assigned to framework aluminum located in the tetrahedral coordination and the octahedral coordinated extra framework aluminum, respectively.[34] After steam treatment, a new resonance centered at around 32 ppm can be detected, corresponding to penta-coordinated extra framework aluminum.[35] The resonance at 55 ppm exhibited a significant drop with the increase of steam temperature, whereas the intensity of resonance at 32 ppm demonstrated an obvious increase. This implied that steam treatment led to dealumination of tetrahedral coordinated framework aluminum, which had a negative effect on the stability of the framework aluminum species. Just as Aukett *et al.*[36] reported, rearrangement and removal of the framework aluminum species to extra framework aluminum can be induced by high-temperature steam. Moreover, a decrease of resonance at 0 ppm with increasing steam temperature indicated a lower proportion of classical octahedral coordinated aluminum.

Fig. 4b shows the ^{27}Al MAS NMR spectra of phosphorus modified ZSM-5 samples. In comparison with the unmodified HZ sample, two newly broad resonances at around the 39, −12 ppm and a weak resonance at 10 ppm could be identified after phosphorus modification. The resonance at 39 and −12 ppm are usually assigned to distorted tetrahedral coordinated framework aluminum and octahedral coordinated aluminum interacting with phosphorus species, respectively.[37] The resonance at 10 ppm corresponds to penta-coordinated framework aluminum associated with phosphorus species.[38] As the P/Al ratio increased, a remarkable decrease of the resonance at 55 ppm could be observed accompanied with a notable increase of the resonance at 39 ppm and a slight increase of the resonance at 10 ppm, indicating the transformation of the tetra-coordinated aluminum mainly into distorted tetra-coordinated during the process of phosphorus modification. In addition, the resonance at −12 ppm became larger while the resonance at 0 ppm decreased gradually due to the interaction of phosphorus species.

Fig. 5 illustrates ^{31}P MAS NMR spectra of phosphorus modified ZSM-5 samples. Four resonances at around 0, −6, −30 and −40 ppm can be detected after phosphorus treatment. The resonances centered at 0, −6 ppm are usually attributed to free monomeric orthophosphate and pyrophosphates, or terminal groups in short polyphosphate chains, respectively.[39] The resonances centered at −30, −40 ppm are related to bidentate and highly condensed phosphates, respectively.[37] An increase of the resonances at 0, −6 and 30 ppm can be observed with a decrease of the resonance at −40 ppm as the P/Al ratio increased, indicating a higher proportion of free monomeric orthophosphate to bidentate phosphate species.

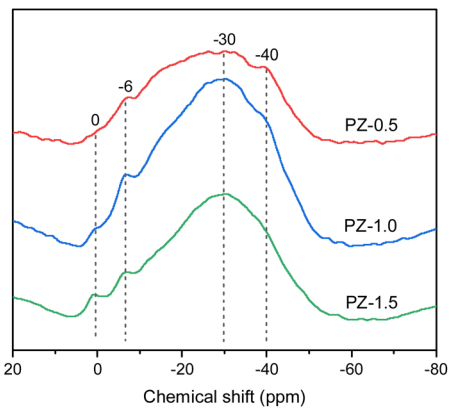

Fig. 5 ^{31}P MAS NMR spectra of phosphorus modified ZSM-5 samples.

3.2 Ethylene oligomerization over steam modified ZSM-5 samples

We investigated the catalytic performance of steam modified ZSM-5 samples in ethylene oligomerization. As shown in Fig. 6a, the unmodified HZ sample showed an ethylene conversion of approximately 100% for 4 h on stream. After steam treatment, both the initial conversion at 1 h and the overall conversion decreased to some extent. The HZ-600 sample maintained nearly full conversion during 4 h on stream. A slight decline in initial conversion can be observed over the HZ-700 sample and around 95% of ethylene conversion was obtained at the end of the test. As the steam temperature increased higher than 700 °C, the HZ-750 sample showed around 87% ethylene conversion at the earlier 1 h that declined significantly to around 40% after 4 h on stream, indicating an obvious deactivation. Furthermore,

© 2025 The Author(s). Published by the Royal Society of Chemistry

Open Access Article. Published on 28 March 2025. Downloaded on 12/14/2025 8:48:57 AM.
This article is licensed under a Creative Commons Attribution-NonCommercial 3.0 Unported Licence.

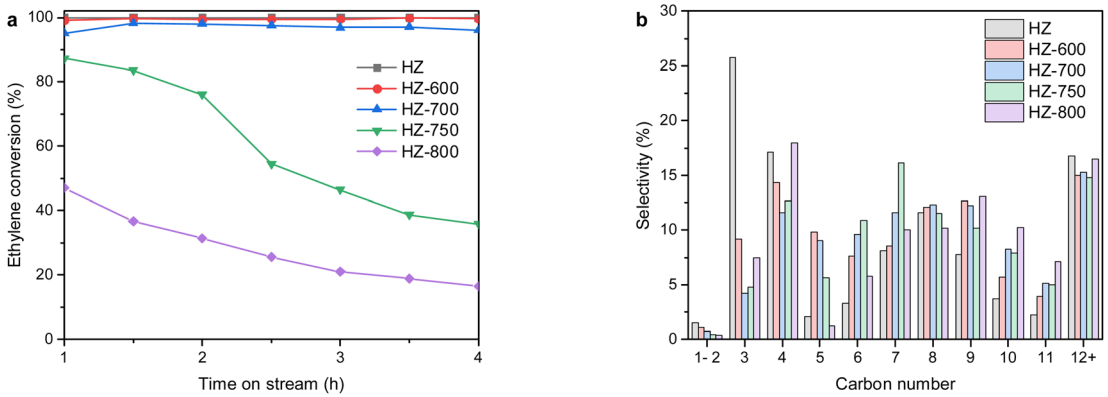

Fig. 6 (a) Evolution of ethylene conversion and (b) product distribution of carbon number with time on stream of 4 h over steam modified ZSM-5 samples.

a poor performance was observed over the HZ-800 sample that the ethylene conversion dropped steadily from approximately 47% to 16% within 4 h on stream. This result demonstrated the significant role of total acidity on the activity, which has been reported in the oligomerization of butylene over HZSM-5 zeolites with different SiO_2/Al_2O_3 ratios.[40]

The product distribution of carbon number over steam modified ZSM-5 samples is shown in Fig. 6b. Compared with the unmodified HZ sample, the selectivity to C_3 hydrocarbons decreased significantly with a less pronounced decrease in selectivity to C_4 hydrocarbons when the steam temperature elevated in the range of 600–700 °C. The selectivity to C_5–C_8 products increased steadily at the same time. As the temperature increased further from 750 to 800 °C, a notable enhancement in distribution of C_3–C_4 hydrocarbons and a drop in selectivity towards C_5–C_8 hydrocarbons can be observed. In addition, the distribution of C_{10}–C_{11} hydrocarbons increased as with the temperature, especially for the HZ-800 sample. From Table 3, a remarkable drop in the ethylene conversion from 93.5% to 43.2% occurred for HZ-700 and HZ-750, respectively. In comparison with the unmodified HZ sample, the selectivity to C_1–C_4 hydrocarbons firstly decreased significantly from 44.4% to 16.5% when the steam temperature elevated in the range of 600 to 700 °C, and then increased to 25.8% as the temperature increased further to 800 °C. Concurrently, the maximum selectivity to C_5–C_{11} hydrocarbons (68.2%) can be obtained over the HZ-700 sample. The HTC (Hydrogen Transfer Coefficient) greatly decreased from 87.9 to 0.3 as the steam temperature increased at 600–800 °C, which was consistent with trend of the selectivity to BTX. To sum up, the HZ-700 sample exhibited the highest selectivity to liquid products up to 83.5% with an ethylene conversion of 93.5%.

3.3 Ethylene oligomerization over phosphorus modified ZSM-5 samples

The catalytic performance of phosphorus modified ZSM-5 samples was also evaluated under the same reaction conditions, and the results are shown in Fig. 7 and Table 3. From Fig. 7a, an increase of the P/Al ratio up to 1.0 gave rise to an unnoticeable decrease in the initial and overall ethylene conversion compared with the pristine HZ sample. While, an obvious drop in ethylene conversion can be observed when the P/Al ratio increased further to 1.5. The PZ-1.5 sample showed around 96% of ethylene conversion at the earlier 1 h that declined significantly to around 20% after 4 h on stream, indicating the occurrence of a fast deactivation.

As shown in Fig. 7b, compared with the unmodified HZ sample, the selectivity to C_3 hydrocarbons decreased

Table 3 Catalytic activity of ethylene oligomerization over steam and phosphorus modified ZSM-5 samples[a]

		Selectivity (wt%)					
Sample	Ethylene conversion (wt%)	C_1–C_4	C_5–C_{11}	C_{12+}	BTX	Liquid	HTC
HZ	99.9	44.4	38.9	16.7	16.5	55.6	87.9
HZ-600	99.2	24.7	60.3	15.0	9.6	75.3	29.0
HZ-700	93.5	16.5	68.2	15.3	2.2	83.5	2.0
HZ-750	43.2	17.9	67.3	14.8	1.8	82.1	0.4
HZ-800	20.0	25.8	57.7	16.5	1.2	74.2	0.3
PZ-0.5	99.6	41.0	43.1	15.9	15.8	59.0	67.5
PZ-1.0	95.8	22.5	64.6	12.9	7.8	77.5	6.3
PZ-1.5	34.8	20.5	60.9	18.6	4.3	79.5	0.4

[a] Reaction conditions: $P = 20$ bar, $T = 300$ °C, TOS = 4 h, WHSV = 1.0 h^{-1}. BTX: benzene, toluene and xylene. HTC (Hydrogen Transfer Coefficient) = $(S(C_3H_8) + S(C_4H_{10}))/(S(C_3H_6) + S(C_4H_8))$.

© 2025 The Author(s). Published by the Royal Society of Chemistry

Open Access Article. Published on 28 March 2025. Downloaded on 12/14/2025 8:48:57 AM.
This article is licensed under a Creative Commons Attribution-NonCommercial 3.0 Unported Licence.

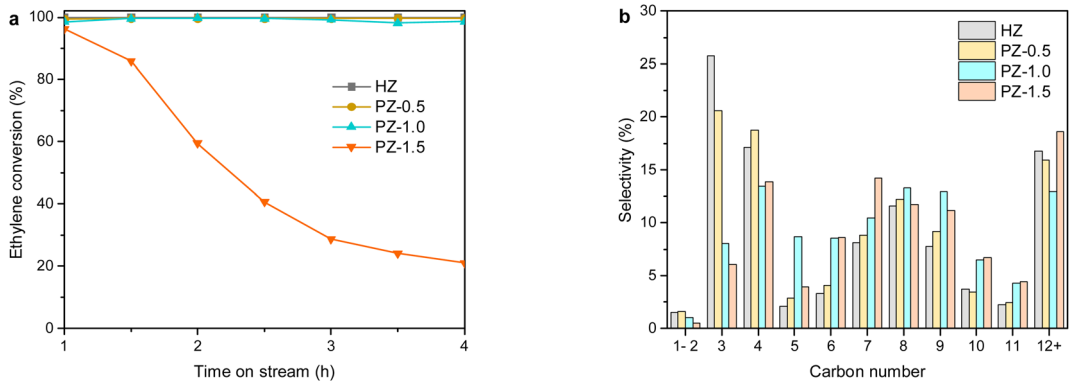

Fig. 7 (a) Evolution of ethylene conversion and (b) product distribution of carbon number with time on stream of 4 h over phosphorus modified ZSM-5 samples.

significantly over phosphorus modified samples, while the selectivity to C_5–C_9 hydrocarbons enhanced steadily when the P/Al ratio increased in the range of 0–1.0. As this ratio increased further to 1.5, the product distribution shifted to larger C_{10}–C_{12} hydrocarbons and a drop in selectivity toward C_5 and C_8 hydrocarbons can be observed. From Table 3, a marked decrease in the ethylene conversion from 95.8% to 34.8% occurred for PZ-1.0 and PZ-1.5, respectively. The selectivity to C_1–C_4 hydrocarbons steadily decreased from 44.4% for HZ to 20.5% for PZ-1.5 with an increase of liquid selectivity up to 79.5% for PZ-1.5. The selectivity to C_5–C_{11} fraction presented volcano-type relationship with an increase of P/Al ratio, and PZ-1.0 showed the highest selectivity to C_5–C_{11} hydrocarbons. Differently, larger P/Al ratio led to a higher distribution of C_{12+} products over the PZ-1.5 sample. In addition, the HTC greatly decreased from 87.9 to 0.4, which was also consistent with trend of the BTX. In total, the PZ-1.0 sample demonstrated a relatively higher selectivity to liquid fuel-range products with a superior activity.

3.4 Discussion

As described above, steam and phosphorus treatment could significantly influence the pore structure and acid properties detected by comprehensive characterization with XRD, XPS, N_2 physisorption, NH_3-TPD, Py-IR and MAS NMR. As shown in Fig. 2b, steam modified ZSM-5 samples generated mesopores with pore diameter in the range of 2–3 nm and 10–20 nm and preserved mostly microporous structure at the same time. Removal of tetrahedral coordinated framework aluminum occurred during the process of steam treatment, which in turn led to an obvious decline in total acidity and acid strength, especially when steam temperature was higher than 700 °C. On the other hand, the presence of free monomeric orthophosphate to bidentate phosphates species was observed in the exterior surface of ZSM-5 zeolites (Fig. 5), which resulted in the blockage of zeolite channels. Therefore, a sharp decrease of the BET surface area and micropore volume can be identified as the P/Al ratio increased. The interaction between the phosphorus species and the zeolite framework gave rise to the transformation of the tetra-coordinated aluminum. Concurrently, a decline in total acidity and the number of strong acid sites was observed with an increase in the P/Al ratio, especially for the PZ-1.5 sample. The subsequent evaluation results prompted further exploration of the roles of the pore structure and acid property in catalytic performance over the steam and phosphorus modified ZSM-5 samples.

In order to explain the differences in activity and product distribution over steam and phosphorus modified ZSM-5 samples, the recognition of reaction pathways for ethylene oligomerization is essential. It is generally accepted that ethylene oligomerization to liquid products over acid catalysts proceeds *via* the classic carbenium-ion chemistry.[41,42] Simplified reaction pathways for ethylene oligomerization over zeolite catalysts are depicted in Scheme 1. The reaction cycle is initiated by the activation of ethylene, which then dimerizes to

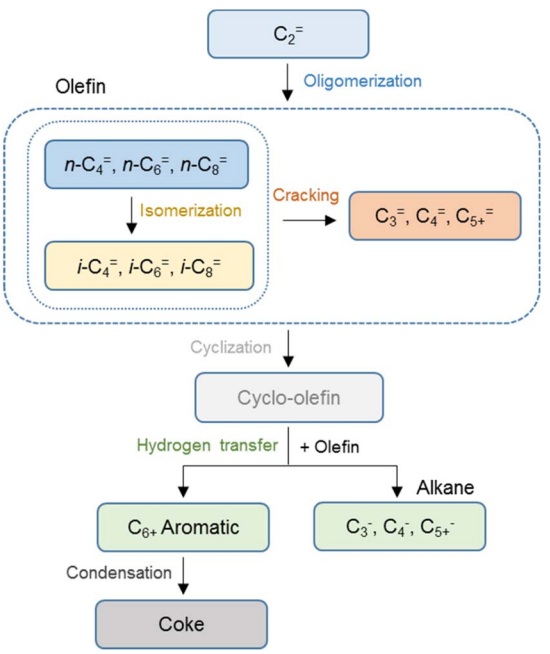

Scheme 1 Simplified reaction pathways for ethylene oligomerization over zeolite catalysts.

© 2025 The Author(s). Published by the Royal Society of Chemistry

Open Access Article. Published on 28 March 2025. Downloaded on 12/14/2025 8:48:57 AM.
This article is licensed under a Creative Commons Attribution-NonCommercial 3.0 Unported Licence.

produce a C_4 carbenium ion. The formed carbenium ion will prefer to isomerize and yield more stable secondary or tertiary carbenium ion, which could oligomerize to form larger C_{6+} hydrocarbons or desorb to produce C_4 olefin. At the same time, other parallel reaction steps occur, such as cracking, hydrogen transfer, cyclization and condensation. The cracking of larger carbenium ions tends to yield C_{3+} olefins and minor carbenium ions, whereas hydrogen transfer between olefin and cyclo-olefin results in the formation of alkane and aromatic. In addition, C_{3+} olefin could easily cyclize to generate highly unstable cyclo-olefin, which undergoes rapid condensation to yield aromatic and poly-aromatic hydrocarbons, or even coke.

The acid property and pore structure of ZSM-5 samples are crucial factors in determining the relative contribution of the aforementioned reaction pathways.[43] As ethylene predominantly reacted on the most acidic sites,[44] the initial ethylene conversion at 1 h on stream decreased steadily, consistent with a decline in the strong Brønsted acid sites (Fig. S2†). Once olefins were formed *via* the oligomerization and isomerization, the successive cracking and hydrogen transfer reactions would influence the product distribution. Due to a decline in total acidity after steam and phosphorus treatment, the modified ZSM-5 samples showed a lower conversion in comparison with the pristine HZ sample. The cracking reactions generally take place at relatively high conversion levels. Therefore, a reduction in cracking was observed over steam and phosphorus modified samples, which contributed to an obvious decrease in the selectivity to C_1–C_4 hydrocarbons. When steam temperature was higher than 700 °C or the P/Al ratio was larger than 1.0, the

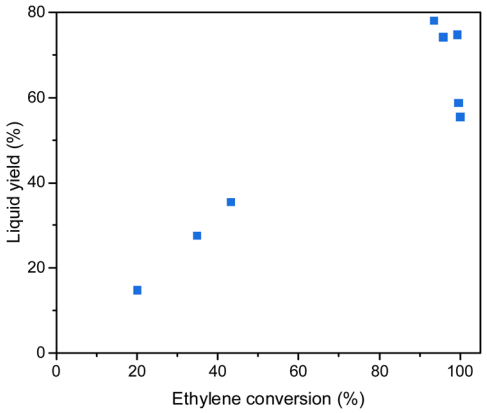

Fig. 9 Liquid yield as a function of ethylene conversion over steam and phosphorus modified ZSM-5 samples.

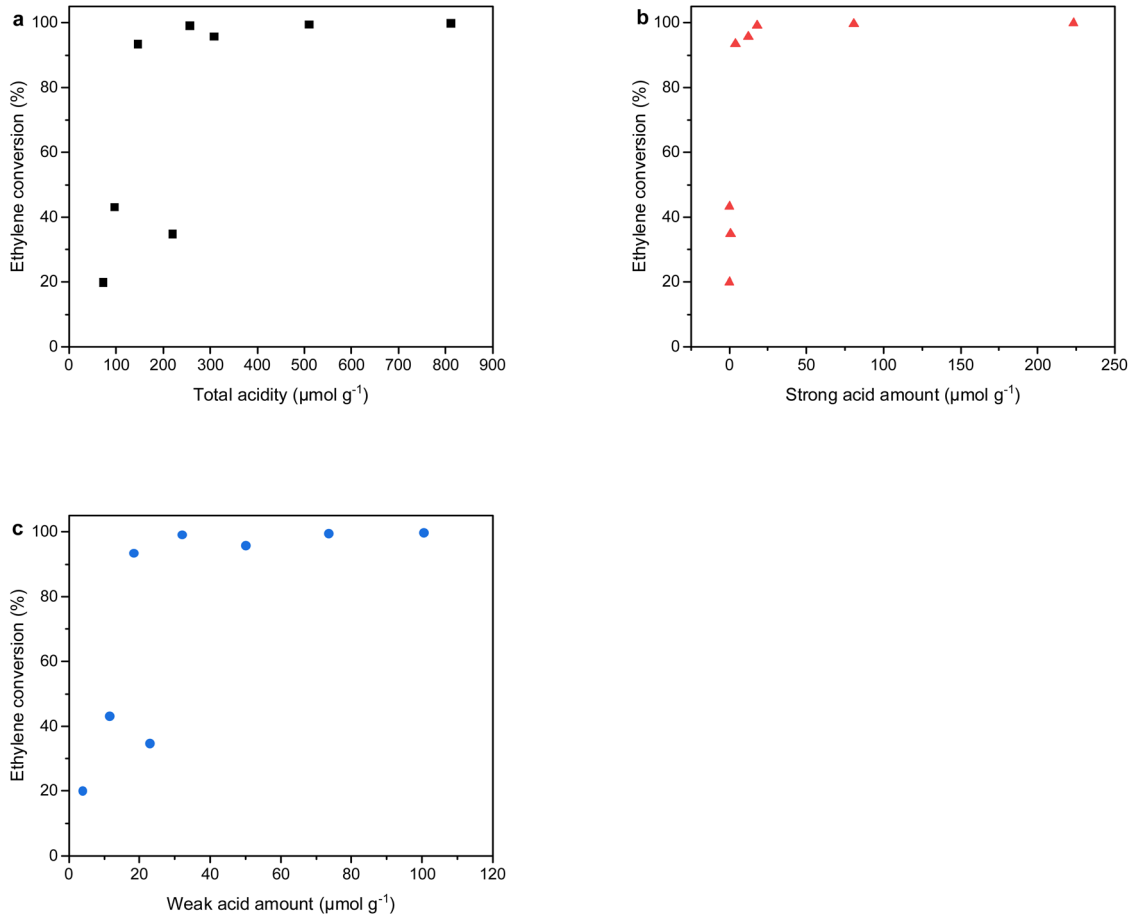

Fig. 8 Ethylene conversion as a function of (a) total acidity, (b) strong acid amount and (c) weak acid amount over steam and phosphorus modified ZSM-5 samples.

Open Access Article. Published on 28 March 2025. Downloaded on 12/14/2025 8:48:57 AM.
This article is licensed under a Creative Commons Attribution-NonCommercial 3.0 Unported Licence.

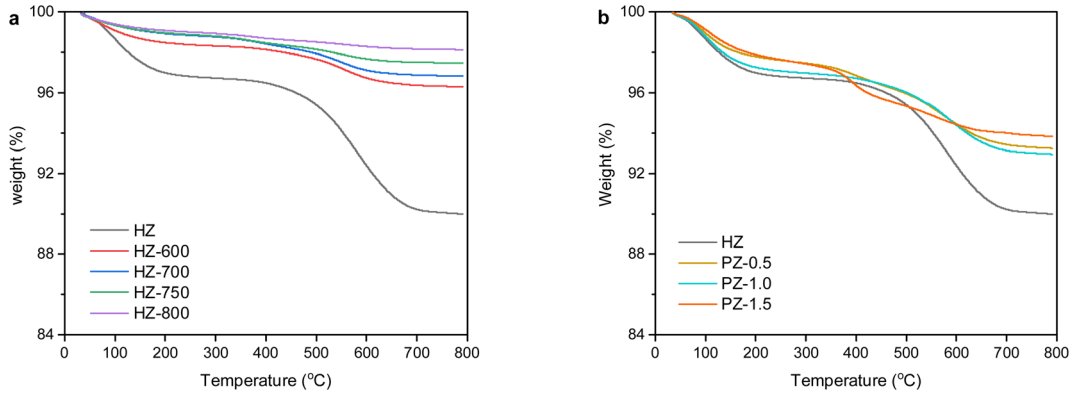

Fig. 10 TG curves of the spent (a) steam and (b) phosphorus modified ZSM-5 samples.

modified ZSM-5 samples quickly lost its activity during 4 h on stream because of a significant drop in number of total acidity, especially the strong acid sites. The lower conversion promoted the initial dimerization pathway, which was beneficial to the formation of C_4 products.[45] On the other hand, more high-carbon products were retained over HZ-700, HZ-800 and PZ-1.5 due to a decline in subsequent cracking reactions. Since hydrogen transfer reactions are commonly catalyzed by catalysts with a high concentration of acid sites.[46] Therefore, the lower propensity for hydrogen transfer reactions over the modified ZSM-5 samples resulted in a decline in selectivity towards BTX products as the total acidity decreased. Interestingly, when steam modified samples were compared with the phosphorus treated ZSM-5 samples, the total acidity of PZ-1.5 (219.2 μmol g^{-1}) was higher than that of the HZ-700 sample (146.0 μmol g^{-1}). However, the ethylene conversion of the PZ-1.5 sample (34.8%) was much lower than that of HZ-700 (93.5%). Corma *et al.*[47] reported that the available Brønsted acid sites on the inner pore of MFI zeolite was crucial for propylene oligomerization. Our results suggested that the mesopores of the HZ-700 sample could favor the accessibility to active sites, while the evident aggregation of phosphorus species on the exterior surface exerted limitations on reactant molecules.

We further studied the relationship between ethylene conversion with the total acidity, the amount of strong acid sites and weak acid sites, and the results are shown in Fig. 8. It was obvious that the strong acid sites demonstrated a fairly better correlation with the ethylene conversion in comparison with the total acidity and weak acid sites. It proved the significance of strong acid sites in ethylene conversion, which was consist with the previous studies.[48,49] The ethylene conversion and liquid yield as a function of mesopore volume are shown in Fig. S3.† The mesopore volume presented a poor relationship with the ethylene conversion and liquid yield. In addition, the liquid yield as a function of ethylene conversion is plotted and displayed in Fig. 9. It was clear that approximately 90–95% ethylene conversion was beneficial to the liquid product. The HZ-700 sample obtained the maximum liquid yield up to 78.1%, which demonstrated an increase of approximately 40% in comparison with the unmodified HZ sample.

Table 4 Coke content of the spent ZSM-5 samples

Sample	Coke content (%)
HZ	7.0
HZ-600	2.2
HZ-700	2.1
HZ-750	1.5
HZ-800	0.9
PZ-0.5	4.5
PZ-1.0	4.3
PZ-1.5	4.0

To investigate the catalyst deactivation, the TG curves of spent steam and phosphorus modified ZSM-5 samples are shown in Fig. 10 and summarized in Table 4. Compared with the unmodified HZ sample, steam and phosphorus modified ZSM-5 samples showed a notable lower coke content. More specifically, steam modified samples exhibited a much lower coke content than the phosphorus modified samples at relatively similar conversion levels. The coke content of HZ-700 (2.1%) was nearly half of that for PZ-1.0 (4.3%). These results were partly attributed to the lower content of acid sites, which resulted in a reduction of hydrogen transfer reactions. On the other hand, the mesopores with larger pore diameter of 2–3 nm and 10–20 nm in the steam modified samples were beneficial in alleviating diffusional limitations, which contributed to an enhanced mass transfer rate. A higher deactivation stability has also been reported in conversion of *n*-butanol/acetone mixtures over ZSM-5 zeolites,[50] which could be related to the formation of a secondary mesopore structure by dealumination treatment.

4. Conclusions

In this work, we have shown that steam and phosphorus modification of ZSM-5 zeolites could improve the yield of liquid fuels and alleviate catalyst deactivation in ethylene oligomerization. A series of modified ZSM-5 samples were prepared under different steam temperature of 600–800 °C or with P/Al ratio of 0–1.5. Characterization results showed that new mesopores with pore diameter of 2–3 nm and 10–20 nm were generated

© 2025 The Author(s). Published by the Royal Society of Chemistry

Open Access Article. Published on 28 March 2025. Downloaded on 12/14/2025 8:48:57 AM. This article is licensed under a Creative Commons Attribution-NonCommercial 3.0 Unported Licence.

after steam treatment. While progressive deposition of phosphorus species on the exterior surface led to notable blockage of zeolite channels over phosphorus modified ZSM-5 samples. Removal of tetrahedral coordinated framework aluminum after steam and phosphorus modification resulted in a gradual decline in total acidity and strong acid sites with the increase of steam temperature or P/Al ratio. These results demonstrated that strong acid sites and accessibility to the inner channel were crucial to production of liquid fuels and coke content. The HZ-700 sample obtained the highest yield of liquid fuels up to 78.1%, which showed an increase of 40% than that of the unmodified HZ sample. Furthermore, HZ-700 sample also exhibited a superior deactivation stability compared with the PZ-1.0 at similar ethylene conversion levels. Our results would provide some insight into the design of zeolite-based catalysts applied in production of liquid fuels from ethylene oligomerization.

Data availability

The authors confirm that the data supporting the findings of this study are available within the article.

Author contributions

Fuchao Li: methodology, data curation, formal analysis, investigation, writing – original draft. Jianqiang Liu: formal analysis, investigation, data curation. Enhui Xing: resources, writing – review & editing. Xiaoli Wei: resources. Jianhong Gong: funding acquisition, writing – review & editing. Yibin Luo: supervision, project administration. Xingtian Shu: conceptualization, supervision.

Conflicts of interest

There are no conflicts to declare.

Acknowledgements

This work was supported by the National Key R&D Program of China (2021YFA1501200) and Sinopec Research Program (KL123001).

Notes and references

1 C. P. Nicholas, *Appl. Catal.*, 2017, **543**, 82–97.
2 E. Koninckx, P. S. F. Mendes, J. W. Thybaut and L. J. Broadbelt, *Appl. Catal., A*, 2021, **624**, 118296.
3 H. Olivier-Bourbigou, P. A. R. Breuil, L. Magna, T. Michel, M. F. Espada Pastor and D. Delcroix, *Chem. Rev.*, 2020, **120**, 7919–7983.
4 A. Gagliardi, G. Balestra, J. De Maron, R. Mazzoni, T. Tabanelli and F. Cavani, *Appl. Catal., B*, 2024, **349**, 123865.
5 V. Hulea, *ACS Catal.*, 2018, **8**, 3263–3279.
6 W. Keim, *Angew. Chem., Int. Ed.*, 2013, **52**, 12492–12496.
7 P. Pletcher, A. Welle, A. Vantomme and B. M. Weckhuysen, *J. Catal.*, 2018, **363**, 128–135.
8 G. Tembe, *Catal. Rev.*, 2022, **65**, 1412–1467.
9 L. Chen, G. Li, Z. Wang, S. Li, M. Zhang and X. Li, *Catalysts*, 2020, **10**, 180.
10 M. Lee, J. W. Yoon, Y. Kim, J. S. Yoon, H.-J. Chae, Y.-H. Han and D. W. Hwang, *Appl. Catal., A*, 2018, **562**, 87–93.
11 A. Martínez Gómez-Aldaraví, C. Paris, M. Moliner and C. Martínez, *J. Catal.*, 2023, **426**, 140–152.
12 A. Ehrmaier, Y. Liu, S. Peitz, A. Jentys, Y.-H. C. Chin, M. Sanchez-Sanchez, R. Bermejo-Deval and J. Lercher, *ACS Catal.*, 2019, **9**, 315–324.
13 S. Moon, H.-J. Chae and M. B. Park, *Appl. Catal., A*, 2018, **553**, 15–23.
14 R. D. Andrei, E. Borodina, D. Minoux, N. Nesterenko, J.-P. Dath, C. Cammarano and V. Hulea, *Ind. Eng. Chem. Res.*, 2020, **59**, 1746–1752.
15 S. Moussa, P. Concepción, M. A. Arribas and A. Martínez, *Appl. Catal., A*, 2020, **608**, 117831.
16 R. Beucher, V. Hulea and C. Cammarano, *React. Chem. Eng.*, 2022, **7**, 133–141.
17 H. O. Mohamed, V. K. Velisoju, I. Hita, O. Abed, R. K. Parsapur, N. Zambrano, M. B. Hassine, N. Morlanes, A.-H. Emwas, K.-W. Huang and P. Castaño, *Chem. Eng. J.*, 2023, **475**, 146077.
18 R. Joshi, G. Zhang, J. T. Miller and R. Gounder, *ACS Catal.*, 2018, **8**, 11407–11422.
19 Z. N. Lashchinskaya, A. A. Gabrienko, A. A. Kolganov, E. A. Pidko and A. G. Stepanov, *J. Phys. Chem. C*, 2022, **126**, 6570–6577.
20 Y. Ganjkhanlou, G. Berlier, E. Groppo, E. Borfecchia and S. Bordiga, *Top. Catal.*, 2017, **60**, 1664–1672.
21 F. Jin, P. Zhang and G. Wu, *Chem. Eng. Sci.*, 2021, **229**, 116144.
22 G. Chen, H. Liu, S. Fadaeerayeni, J. Shan, A. Xing, J. Cheng, H. Wang and Y. Xiang, *Catal. Sci. Technol.*, 2020, **10**, 4019–4029.
23 S. M. T. Almutairi, B. Mezari, E. A. Pidko, P. C. M. M. Magusin and E. J. M. Hensen, *J. Catal.*, 2013, **307**, 194–203.
24 Z. Xu, T. Fu, Y. Han, Z. Li and G. Zhan, *Fuel*, 2023, **349**, 128671.
25 C. S. Triantafillidis, A. G. Vlessidis, L. Nalbandian and N. P. Evmiridis, *Microporous Mesoporous Mater.*, 2001, **47**, 369–388.
26 B. Lin, Q. Zhang and Y. Wang, *Ind. Eng. Chem. Res.*, 2009, **48**, 10788–10795.
27 H. L. Janardhan, G. V. Shanbhag and A. B. Halgeri, *Appl. Catal., A*, 2014, **471**, 12–18.
28 L. Guan, C. Huang, D. Han, L. Zhu, Y. Mei, D. He and Y. Zu, *Microporous Mesoporous Mater.*, 2022, **330**, 111605.
29 J. A. Lercher and G. Rumplmayr, *Appl. Catal.*, 1986, **25**, 215–222.
30 K. A. Cychosz, R. Guillet-Nicolas, J. García-Martínez and M. Thommes, *Chem. Soc. Rev.*, 2017, **46**, 389–414.
31 Y.-J. Lee, J. M. Kim, J. W. Bae, C.-H. Shin and K.-W. Jun, *Fuel*, 2009, **88**, 1915–1921.

© 2025 The Author(s). Published by the Royal Society of Chemistry

Open Access Article. Published on 28 March 2025. Downloaded on 12/14/2025 8:48:57 AM.
This article is licensed under a Creative Commons Attribution-NonCommercial 3.0 Unported Licence.

32 E. Catizzone, A. Aloise, E. Giglio, G. Ferrarelli, M. Bianco, M. Migliori and G. Giordano, *Catal. Commun.*, 2021, **149**, 106214.
33 C. A. Emeis, *J. Catal.*, 1993, **141**, 347–354.
34 L. Rodríguez-González, F. Hermes, M. Bertmer, E. Rodríguez-Castellón, A. Jiménez-López and U. Simon, *Appl. Catal., A*, 2007, **328**, 174–182.
35 T. Blasco, A. Corma and J. Martínez-Triguero, *J. Catal.*, 2006, **237**, 267–277.
36 P. N. Aukett, S. Cartlidge and I. J. F. Poplett, *Zeolites*, 1986, **6**, 169–174.
37 H. E. van der Bij, L. R. Aramburo, B. Arstad, J. J. Dynes, J. Wang and B. M. Weckhuysen, *ChemPhysChem*, 2014, **15**, 283–292.
38 M. Göhlich, W. Reschetilowski and S. Paasch, *Microporous Mesoporous Mater.*, 2011, **142**, 178–183.
39 K. Damodaran, J. W. Wiench, S. M. Cabral de Menezes, Y. L. Lam, J. Trebosc, J. P. Amoureux and M. Pruski, *Microporous Mesoporous Mater.*, 2006, **95**, 296–305.
40 M. Díaz, E. Epelde, Z. Tabernilla, A. Ateka, A. T. Aguayo and J. Bilbao, *Energy*, 2020, **207**, 118317.
41 J. S. Buchanan, J. G. Santiesteban and W. O. Haag, *J. Catal.*, 1996, **158**, 279–287.
42 G. Bellussi, F. Mizia, V. Calemma, P. Pollesel and R. Millini, *Microporous Mesoporous Mater.*, 2012, **164**, 127–134.
43 S. Moussa, M. A. Arribas, P. Concepción and A. Martínez, *Catal. Today*, 2016, **277**, 78–88.
44 I. Hita, H. O. Mohamed, Y. Attada, N. Zambrano, W. Zhang, A. Ramírez and P. Castaño, *Catal. Sci. Technol.*, 2023, **13**, 1288–1300.
45 K. Toch, J. W. Thybaut, M. A. Arribas, A. Martínez and G. B. Marin, *Chem. Eng. Sci.*, 2017, **173**, 49–59.
46 A. Corma, P. J. Miguel and A. V. Orchilles, *J. Catal.*, 1994, **145**, 171–180.
47 A. Corma, C. Martínez and E. Doskocil, *J. Catal.*, 2013, **300**, 183–196.
48 X. Wang, X. Hu, C. Song, K. W. Lux, M. Namazian and T. Imam, *Ind. Eng. Chem. Res.*, 2017, **56**, 12046–12055.
49 D. Nozik and A. T. Bell, *ACS Catal.*, 2022, **12**, 14173–14184.
50 A. de Lucas, P. Canizares, A. Durán and A. Carrero, *Appl. Catal., A*, 1997, **154**, 221–240.

© 2025 The Author(s). Published by the Royal Society of Chemistry